Petroleum Science 23 (2026) 2976–2990

Contents lists available at ScienceDirect

Petroleum Science

journal homepage: www.keaipublishing.com/en/journals/petroleum-science

Original Paper

Advancing CCUS-EOR in low-permeability reservoirs with surfactant-enhanced carbonated water and CO_2 alternating flooding: An integrated experimental and numerical investigation

Xiao-Bing Han [a], Hai-Yang Yu [a,*], Tong-Bing Wang [a], Peng Song [b], Jia-Bang Song [a], Lu Liu [a], Hui-Ting Tang [a], Jun Lu [c], Yang Wang [a,**]

[a] State Key Laboratory of Petroleum Resources and Engineering, China University of Petroleum (Beijing), Beijing, 102249, China
[b] Research Institute of Exploration and Development, PetroChina Changqing Oilfield Company, Xi'an, Shaanxi, 710018, China
[c] McDougall School of Petroleum Engineering, The University of Tulsa, Tulsa, OK, 74104, USA

ARTICLE INFO

Article history:
Received 20 May 2025
Received in revised form
25 July 2025
Accepted 30 November 2025
Available online 3 December 2025

Edited by Teng Zhu and Min Li

Keywords:
Enhanced water alternating gas
Sweep efficiency
Oil displacement efficiency
CO_2 storage efficiency

ABSTRACT

Surfactant-enhanced carbonated water alternating with CO_2 (SCWAG) flooding, which integrates the advantages of surfactants, carbonated water (CW), and CO_2, has demonstrated significant potential for the development of low-permeability reservoirs. Nonetheless, the underlying mechanisms of SCWAG-enhanced oil recovery require further elucidation. Its CO_2 storage performance and pore-scale oil displacement characteristics have not been thoroughly investigated, and the influence of various factors on SCWAG performance remains poorly understood. This study, for the first time, investigates the pore-scale oil displacement characteristics and CO_2 storage performance of SCWAG by integrating core flooding experiments and nuclear magnetic resonance scanning. An innovative core-scale 3D heterogeneous numerical model was developed using computed tomography scanning and refined via history matching, thereby enabling reliable SCWAG simulation and facilitating reservoir-scale analysis of factors affecting SCWAG performance. The results demonstrate that SCWAG notably improves both sweep efficiency and oil displacement efficiency, achieving higher recovery and CO_2 storage efficiency than other methods. The total recovery reached 76.99%, with individual recoveries of 56.35%, 76.85%, and 87.96% for micropores, mesopores, and macropores, respectively, while the CO_2 storage efficiency is 57.22%. Permeability contrast exerts a significant effect on recovery, whereas CO_2 storage efficiency was primarily influenced by the injection rate and water-to-gas ratio. Moreover, the interaction between the water-to-gas ratio and permeability contrast exerts a substantial impact on both recovery and CO_2 storage efficiency. This study provides novel insights and an in-depth analysis of the SCWAG process, offering practical guidelines for its application in low-permeability reservoirs.

1. Introduction

The large-scale emission of greenhouse gases (e.g., CO_2, methane, water vapor) from human activities has intensified the greenhouse effect, accelerating global warming. As the most concerning anthropogenic greenhouse gas, CO_2 is a critical driver of this phenomenon and thus one of the primary targets for mitigation strategies (Cui et al., 2024; Filonchyk et al., 2024; Zhou et al., 2025). In response, Carbon Capture, Utilization, and Storage (CCUS) technologies have been proposed, among which CO_2 flooding enhanced oil recovery (EOR) represents a pivotal approach. This method not only enhances oil recovery but also facilitates CO_2 sequestration (Gao et al., 2025; Lin et al., 2022; Liu and Rui, 2022). The high solubility of CO_2 in oil reduces oil viscosity, induces volume expansion, and lowers interfacial tension (IFT), resulting in superior displacement efficiency (Bai et al., 2025; Liu et al., 2025; Song et al., 2025). Nevertheless, the significant

* Corresponding author.
** Corresponding author.
E-mail addresses: haiyangyu.cup@139.com (H.-Y. Yu), petroyang@cup.edu.cn (Y. Wang).
Peer review under the responsibility of China University of Petroleum (Beijing).

https://doi.org/10.1016/j.petsci.2025.11.049

Nomenclature

CW	Carbonated water
CT	Computed tomography
EOR	Enhanced oil recovery
IFT	Interfacial tension
NMR	Nuclear magnetic resonance
RSM	Response surface methodology
SCW	Surfactant-enhanced carbonated water
SCWAG	Surfactant-enhanced carbonated water altering with CO_2
WAG	Water altering CO_2
PV	Pore volume

differences in viscosity and density between CO_2 and oil result in an unstable displacement front, increasing the risk of gas breakthrough and ultimately reducing sweep efficiency (Luo et al., 2023).

Sweep efficiency is a critical factor that limits the effectiveness of CO_2 development. Water-alternating-gas (WAG) flooding is an effective method for controlling gas breakthrough and improving sweep efficiency (Afzali et al., 2018). The primary mechanism of this method is the alternating flooding of water and gas slugs, which achieves mobility control, stabilizes the displacement front, increases the flow resistance of CO_2, and compels it to enter low-permeability areas, thereby expanding sweep efficiency (Hao et al., 2016). He et al. (2023) simulated WAG injection in a micromodel, analyzing time-varying fingerings and pattern crossovers under three-phase flow conditions. They observed that pressure difference significantly influenced fingering pattern changes. Furthermore, even a small amount of water notably affected the fingering patterns during WAG flooding. Through micro-numerical simulations, they also discovered that CO_2 dissolution into crude oil could suppress fingering phenomena, and that the resulting reduction in crude oil viscosity could inhibit viscous fingering (He et al., 2024). Wang et al. (2020) conducted microfluidic experiments, and the results demonstrated that compared to CO_2 flooding, WAG improved volumetric sweep efficiency by 32.5%, while oil recovery rose by 23.15%. Meanwhile, core displacement experiments using nuclear magnetic resonance (NMR) by Xiao et al. (2017) revealed that WAG significantly improved EOR performance in small pores, achieving a 4.09% increase compared to CO_2 flooding. Field applications have demonstrated that WAG can increase recovery by 5%–10%, while also effectively storing CO_2. Vo Thanh et al. (2020) performed numerical simulations of the Nam Vang oilfield and demonstrated that, in comparison with CO_2 flooding, WAG improved CO_2 storage efficiency by approximately 25%. Although WAG has yielded positive results, it is prone to water shielding, in which the injected water acts as a barrier, preventing direct contact between the injected CO_2 and oil, thereby reducing displacement efficiency (Dong et al., 2005; Majidaie et al., 2012; Tiffin and Yellig, 1983). Furthermore, while water injection improves sweep efficiency, it may also lead to a reduction in oil displacement efficiency.

Carbonated water (CW) refers to water in which CO_2 is dissolved. It can effectively mitigate the negative effects of water shielding, while also reducing oil viscosity, expanding oil volume, improving wettability, and decreasing IFT (Han et al., 2025; Yu et al., 2020). Consequently, several studies have proposed CW alternating gas (CWAG), which involves the alternating injection of CW and CO_2 to further enhance oil recovery while simultaneously facilitating more effective CO_2 storage. Previous studies by Golkari and Riazi (2018) and Riazi and Golkari (2016) compared the diffusion coefficients of brine/oil/CO_2 and carbonated brine/oil/CO_2 systems and demonstrated that the spreading coefficient for the carbonate brine/oil/CO_2 system was positive and higher than that for the brine/oil/CO_2 system. This positive spreading coefficient, induced by the presence of CO_2 in the brine phase, indicates that CWAG is more effective than WAG in enhancing oil recovery. Numerical simulations of CWAG by Majidaie et al. (2012) showed that CW could minimize the water-shielding effect, thereby improving oil recovery. Moreover, CWAG offers excellent CO_2 storage, as part of the CO_2 remains dissolved in the CW, reducing the risk of leakage and contributing to the safe storage of CO_2 (Seyyedi et al., 2018; Shakiba et al., 2016). Ji et al. (2023) investigated the effects of CWAG on EOR and CO_2 storage through numerical simulations. In comparison with WAG, CWAG led to a 1.4% increase in oil recovery and a 6.7% increase in CO_2 storage efficiency. Although CWAG can improve recovery to some extent, its effects on wettability and IFT reduction are limited and require further enhancement. Surfactant flooding is an effective EOR method that significantly reduces IFT while improving wettability. Therefore, adding surfactants to CW can further improve its performance (Nowrouzi et al., 2020; Yu et al., 2019). Alabdulbari et al. (2022) added ionic surfactants to low salinity CW, resulting in a significant reduction in IFT, which remained effective even under high-salinity conditions. Yu et al. (2021) conducted core displacement experiments, which showed that surfactant-enhanced CW (SCW) combined the advantages of both CW and surfactants, improving oil recovery by 23.83%. Chen et al. (2021) drew similar conclusions, indicating that compared to waterflooding followed by CW flooding, the combination of CW and surfactants after waterflooding significantly reduced IFT and achieved higher oil recovery.

Given the advantages of CW and surfactants, SCW alternating with CO_2 flooding (SCWAG) has been introduced. In this approach, SCW replaces the water in conventional WAG, and its injection alternates with CO_2. SCWAG integrates the benefits of CW, surfactants, and CO_2 (Yu et al., 2021; Zhang et al., 2023). Compared to WAG, SCWAG can overcome the negative effects of water shielding and facilitate the transfer of CO_2 into oil. Compared to CWAG, it is more effective at reducing IFT and improving wettability. Shu et al. (2014) conducted core displacement experiments and demonstrated that using CW/SCW as a pre-flush before CO_2 flooding significantly improved oil recovery, with SCW yielding superior results. The primary mechanism is that SCW improves CO_2 transfer efficiency from the aqueous phase to the oil phase. Similarly, Yu et al. (2021) evaluated various displacement methods for tight reservoirs and concluded that SCWAG achieved the highest oil recovery, reaching 36.63%, which represented a 13.8% increase compared to WAG flooding. Although SCWAG exhibits considerable potential for application, research on SCWAG remains limited, and the pore-scale displacement mechanism have yet to be elucidated. Furthermore, current studies concentrate on its effect on oil recovery, whereas its performance in CO_2 storage has yet to be investigated in the literature. Additionally, the influence of various factors on the performance of SCWAG in enhancing oil recovery and CO_2 storage remains insufficiently understood, and the interactions of these factors have yet to be assessed.

This study provides a systematic investigation into the efficacy and mechanisms of SCWAG for EOR and CO_2 sequestration. It also analyzes the influence of different parameters on the performance of SCWAG. By integrating core flooding and nuclear magnetic resonance (NMR) scanning, the pore utilization characteristics of SCWAG are investigated, elucidating its mechanisms and impacts on enhancing oil recovery and CO_2 storage. To further analyze the impacts of various factors and their interactions on SCWAG

performance, a core-scale 3D heterogeneous numerical model, constrained by computed tomography (CT) scanning data and history matching, was developed, thereby enabling reliable SCWAG simulation and facilitating reservoir-scale numerical simulations coupled with response surface methodology (RSM). These findings offer novel insights into the research and application of SCWAG, contributing to both EOR and the achievement of CO_2 storage.

2. Core flooding experiments

2.1. Materials

2.1.1. Cores

Core samples were sourced from Daqing Oilfield in China, with a burial depth of approximately 2200 m. After cutting and cleaning, the core length was about 10.0 cm, and the diameter was approximately 2.5 cm. Core porosity and permeability were measured using the QKY-1 porosity measuring device and the PDP-200 permeability device, respectively. Cores with comparable porosity and permeability were selected for experiments, with an average porosity of 15.80% and an average permeability of 14.54 mD. The cores were primarily composed of quartz. Specific petrophysical parameters of the cores are detailed in Table 1.

2.1.2. Oil

Under reservoir conditions of temperature (72 °C) and pressure (25 MPa), the density of the formation oil is 0.709 g/cm^3, and its viscosity is 0.494 mPa·s. Its saturation pressure is 9.532 MPa, with a gas-to-oil ratio of 96.61 m^3/m^3. Stock tank oil from the target reservoir and its associated gas were utilized to prepare live oil, with a gas-to-oil ratio adjusted to match that of the formation oil, for use in the experiments. The specific composition of the oil, as shown in Fig. 1, reveals that light components predominate, with the C_1–C_{15} fractions accounting for 82.76 mol%. The results of slim-tube experiments demonstrate that the minimum miscibility pressure between CO_2 and crude oil is approximately 20.0 MPa under reservoir temperature. Therefore, miscible CO_2 flooding is considered feasible in the target reservoir.

2.1.3. Surfactant

The surfactant used in the experiment was sourced from the oilfield. It is a zwitterionic surfactant capable of withstanding high temperatures and high salinity, significantly improving wettability and reducing IFT. The critical micelle concentration of the surfactant is 0.03 w.t.%, and considering the potential loss of surfactant during the displacement process, a concentration of 0.10 w.t.% was employed in the experiment, which is the same as that used in the oilfield. To shield the hydrogen signal in water and enable the measurement of recovery in pores of different sizes using NMR, 12.0 w.t.% manganese chloride was added to distilled water, which was subsequently used to prepare the surfactant solution. Under the target reservoir temperature conditions, the IFT between the surfactant solution and oil was 0.08 mN/m. After contact with the experimental core, the contact angle decreased from 132.7° to 63.4° (Fig. 2), indicating that the surfactant retains its effectiveness under high-salinity conditions, thereby exhibits robust salt tolerance and wide applicability.

Table 1
Physical parameters of experimental cores.

Core	Length, cm	Diameter, cm	Porosity, %	Permeability, mD
C-1	10.012	2.502	15.80	14.42
C-2	10.016	2.506	15.76	14.56
C-3	10.032	2.504	15.92	14.80
C-4	10.028	2.503	15.70	14.36

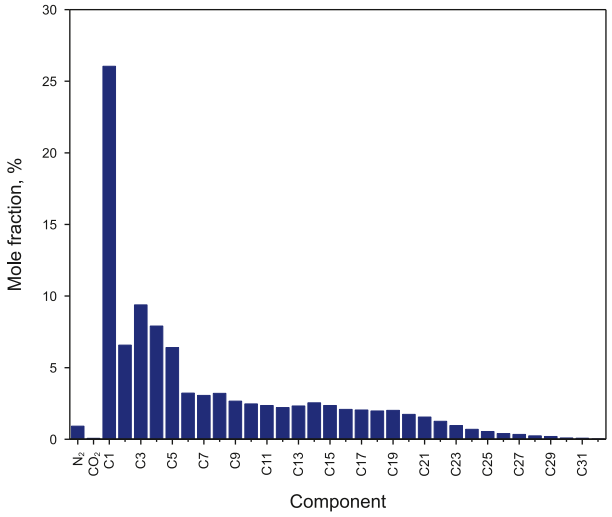

Fig. 1. Composition of formation oil.

2.1.4. Surfactant-enhanced carbonated water

SCW refers to CW supplemented with surfactants, integrating the benefits of both surfactants and CW. A stirrable intermediate container was employed to introduce CO_2 into the surfactant solution; the temperature and pressure were then elevated to the desired levels. The stirring function was subsequently activated to facilitate the dissolution of CO_2. Once the pressure stabilized, stirring was maintained for 24 h to ensure the complete dissolution of CO_2, thereby preparing the SCW. The CO_2 content in the experimental SCW was set to be 1.0 mmol/cm^3.

2.2. Experimental setup and procedure

2.2.1. Experimental setup

Through core flooding experiments, combined with NMR scanning, the oil recovery, CO_2 storage efficiency, and oil displacement characteristics from pores of varying sizes were determined. Fig. 3 illustrates the schematic diagram of the experimental setup, which mainly consists of a constant-rate constant-pressure pump, intermediate containers, a core holder, a back-pressure valve, a gas flow meter, a gas chromatograph, and an NMR scanning system. NMR data were acquired using a MacroMR12-150H-I low-field NMR apparatus. In the experiments, the resonance frequency was 12.448 MHz, the magnetic field strength was 0.3 T, the echo time was 0.2 ms, the polarization time was 3000 ms, and the number of echoes was 12,000.

Additionally, a CT scanner was employed to scan the core samples, and a core-scale 3D heterogeneous numerical simulation model was developed to match the experimental results, validate the reliability of the simulation approach, and derive relative permeability curves for subsequent numerical simulation studies. Specifically, the CT scanning was conducted with a current of 200 mA, a voltage of 120 kV, a scanning layer thickness of 1.25 mm, and a scanning interval of 10.0 mm.

2.2.2. Experimental procedure

The oil and gas production volumes at the core outlet were measured to assess oil recovery and CO_2 storage efficiency. The T_2 spectrum variations before and after displacement were acquired through NMR scanning and utilized to calculate recovery across

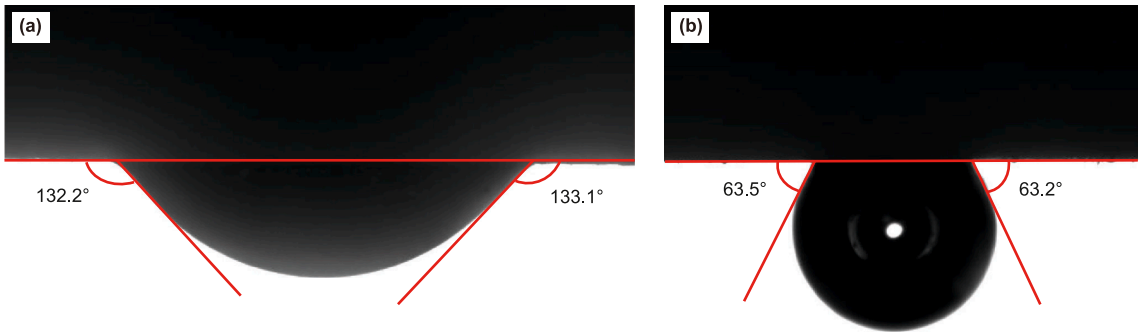

Fig. 2. Comparison of contact angle. **(a)** Before contact with surfactant; **(b)** After contact with surfactant.

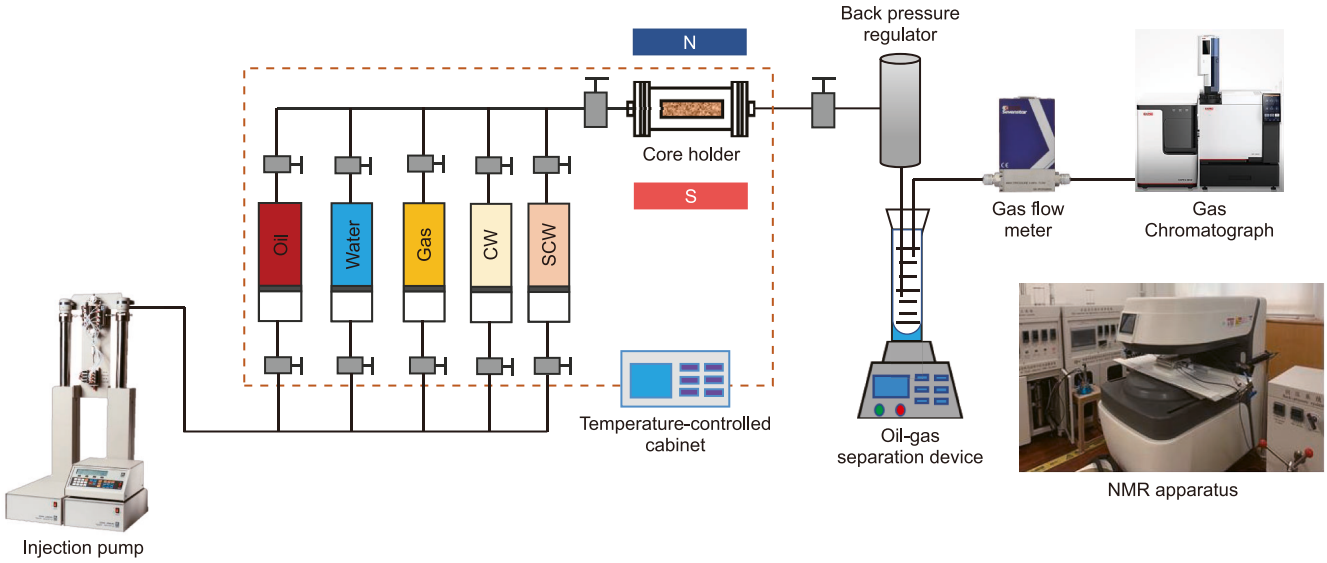

Fig. 3. Schematic diagram of the displacement experimental device.

pores of varying sizes. The specific experimental steps are outlined below:

(1) The core is evacuated for 24 h and then saturated with distilled water for 48 h prior to NMR scanning.
(2) The experimental apparatus is assembled, and a 12 w.t.% manganese chloride solution is injected at a constant flow rate of 0.1 mL/min to suppress the hydrogen signal. After injecting a total of 20 pore volumes, NMR scanning is conducted.
(3) The temperature is adjusted to 72 °C, the pressure to 25 MPa, and the confining pressure is maintained at 3 MPa above the injection pressure. Oil is injected into the core until no water is observed at the outlet, establishing bound water saturation. Subsequently, the core is aged for 72 h and subjected to NMR scanning again.
(4) CO_2 is used to displace the core at a rate of 0.1 mL/min. The injection is terminated after a cumulative volume of 1.2 pore volume (PV) has been injected. Subsequently, an NMR scan is conducted to quantify the oil recovery. During the displacement, oil production is measured at various CO_2 injection volumes to obtain the oil recovery curve. Simultaneously, the produced gas is collected and quantified, and its composition is analyzed via gas chromatography to calculate CO_2 storage efficiency.
(5) The experimental core is replaced; steps (1) to (3) are repeated to re-establish initial conditions, after which WAG, CWAG, and SCWAG flooding is performed as in step (4). For both CWAG and SCWAG flooding experiments, the change in contact angle before and after the experiment is measured using the sessile drop method.

Notably, for both WAG and SCWAG flooding, the slug size is 0.1 PV. Additionally, for the SCWAG experimental core, CT scanning is conducted after evacuation, followed by CT scanning after saturation with experimental water, before displacement experiments are performed. Additionally, certain experimental uncertainties are present. For oil recovery measurements and contact angle determination, the dominant source of error is human-induced, primarily due to reading inaccuracies. For CO_2 storage efficiency, the errors are predominantly systematic, originating from the gas flow meter measurement and chromatographic analysis. Therefore, to account for the influence of these uncertainties, appropriate error bars were added to the experimental data, providing a more comprehensive and accurate representation of the results.

2.3. Quantitative analysis method of NMR

NMR scanning can be employed to obtain the transverse relaxation time distribution spectrum, commonly known as the T_2

spectrum, by detecting NMR signals from hydrogen-containing fluids within porous media. The transverse relaxation time of fluids in porous media is influenced by the combined effects of bulk relaxation, surface relaxation, and diffusion relaxation, which can be expressed as Eq. (1) (Tang et al., 2022; Yang et al., 2013; Zhang et al., 2021):

$$\frac{1}{T_2}=\frac{1}{T_{2,\text{bulk}}}+\frac{1}{T_{2,\text{surface}}}+\frac{1}{T_{2,\text{diffusion}}} \tag{1}$$

where, $T_{2,\text{bulk}}$ is bulk relaxation time, ms; $T_{2,\text{surface}}$ is surface relaxation time, ms; $T_{2,\text{diffusion}}$ is diffusion relaxation time, ms.

For the flow of fluids in porous media, the contribution of $T_{2,\text{bulk}}$ to T_2 is generally minor and can typically be neglected. In low magnetic field environments, $T_{2,\text{diffusion}}$ can also be disregarded. Consequently, T_2 is predominantly influenced by $T_{2,\text{surface}}$, which is related to the specific surface area of the pores and can be expressed as Eq. (2):

$$T_2=T_{2,\text{surface}}=\frac{V}{\rho_t S} \tag{2}$$

where, ρ_t is the surface relaxivity, m/ms; S is the pore surface area, μm^2; V is the pore volume, μm^3.

For porous media, S and V satisfy Eq. (3):

$$\frac{S}{V}=\frac{F_s}{r} \tag{3}$$

where, F_s is shape factor; r is pore radius, μm.

Thus, T_2 can be expressed as Eq. (4):

$$T_2=T_{2,\text{surface}}=\frac{r}{\rho_t F_s} \tag{4}$$

From Eq. (4), it is evident that T_2 is directly proportional to r; that is, a larger T_2 corresponds to a greater r. Based on T_2, pores can be categorized into micropores, mesopores, and macropores, where values less than10 ms correspond to micropores, 10–100 ms to mesopores, and values exceeding 100 ms to macropores. Additionally, the NMR signal intensity is directly proportional to the content of hydrogen-containing fluids within the porous medium. Therefore, the recovery can be determined from variations in the T_2 spectrum as given by Eq. (5):

$$E=\frac{S_1-S_2}{S_1}\times 100\% \tag{5}$$

where, S_1 and S_2 represent the T_2 spectrum peak areas of the oil-saturated core and the core after displacement, respectively.

2.4. Experimental results analysis

2.4.1. Oil recovery

Core samples C-1 to C-4 were utilized to perform CO_2 flooding, WAG flooding, CWAG flooding, and SCWAG flooding experiments, respectively. Fig. 4 depicts the oil recovery curves as a function of injection volume for various displacement methods. Across all displacement methods, recovery increased with injection volume, exhibiting a rapid increase in the initial stage, followed by a more gradual rise in the subsequent stage, attributable to the breakthrough of the injected fluid. SCWAG yielded the highest recovery, reaching 76.99%, representing enhancements of 12.03%, 7.71%, and 4.24% over CO_2 flooding, WAG flooding, and CWAG flooding, respectively.

Fig. 5 illustrates variations in the T_2 spectrum before and after core displacement, while Fig. 6 compares oil recovery across pores

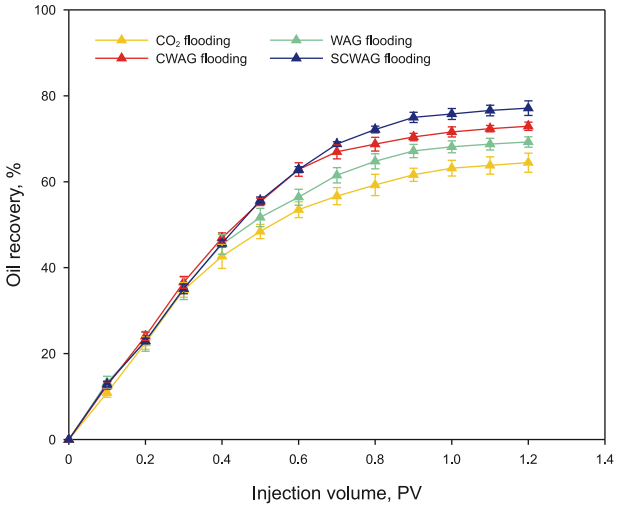

Fig. 4. Recovery variation with injection volume for different displacement methods.

of varying sizes under different displacement methods. The results indicated that SCWAG achieves higher recoveries in micropores, mesopores, and macropores compared with other displacement methods. Under reservoir conditions, CO_2 can attain miscibility with crude oil. Its dissolution in crude oil leads to an expansion of the oil volume and a reduction in viscosity. Experimental results from gas expansion tests showed that the injection of 50 mol% CO_2 into crude oil expanded its volume to 1.308 times the original. Simultaneously, the measured oil viscosity decreased by 43.6%. Additionally, CO_2 contributes to oil displacement through effects like extraction. However, owing to substantial differences in physical properties between CO_2 and oil, gas breakthrough is likely to occur. At a cumulative injection of 1.2 PV, CO_2 flooding yielded a recovery of 64.96%, with recoveries of 38.57%, 66.31%, and 78.72% for micropores, mesopores, and macropores, respectively. WAG flooding, via alternating injections of water and gas slugs, stabilizes the gas displacement front, suppresses gas breakthrough, increases the flow resistance of CO_2, and thereby enhances sweep efficiency (Ren and Duncan, 2021). This approach achieved recoveries of 46.51%, 69.43%, and 81.01% in micropores, mesopores, and macropores, respectively. Compared with WAG flooding, CWAG mitigates the effects of water shielding, promotes the mass transfer of CO_2 into oil, partially breaks the “water shield” effect, and further enhances both sweep efficiency and oil displacement efficiency (Riazi and Golkari., 2016), leading to recoveries of 52.66%, 73.66%, and 82.97% in the corresponding pore categories. SCWAG integrates the respective advantages of surfactants, CW, and CO_2, resulting in EOR across all pore sizes. It achieved recoveries of 56.35% in micropores, 76.85% in mesopores, and 87.96% in macropores. Among these, mesopores and macropores contribute more substantially to recovery, whereas the improvement in recovery for micropores was the most significant.

The mechanisms through which SCWAG improves oil recovery primarily encompass: (1) SCWAG effectively mitigates the effects of water shielding and promotes the mass transfer of CO_2 into oil. As illustrated in Fig. 7, WAG flooding is susceptible to inducing water shielding, with the CO_2 transfer process occurring in the sequence: CO_2-water-oil. In contrast, in SCWAG flooding, CO_2 is pre-dissolved, allowing the CO_2 transfer process to be approximated as SCW- oil. (2) The synergistic effect of the surfactant and CW leads to a more effective improvement in wettability and reduction in IFT. SCW can reduce the IFT between itself and crude oil to 1×10^{-2} mN/m, which is lower than that of CW and oil

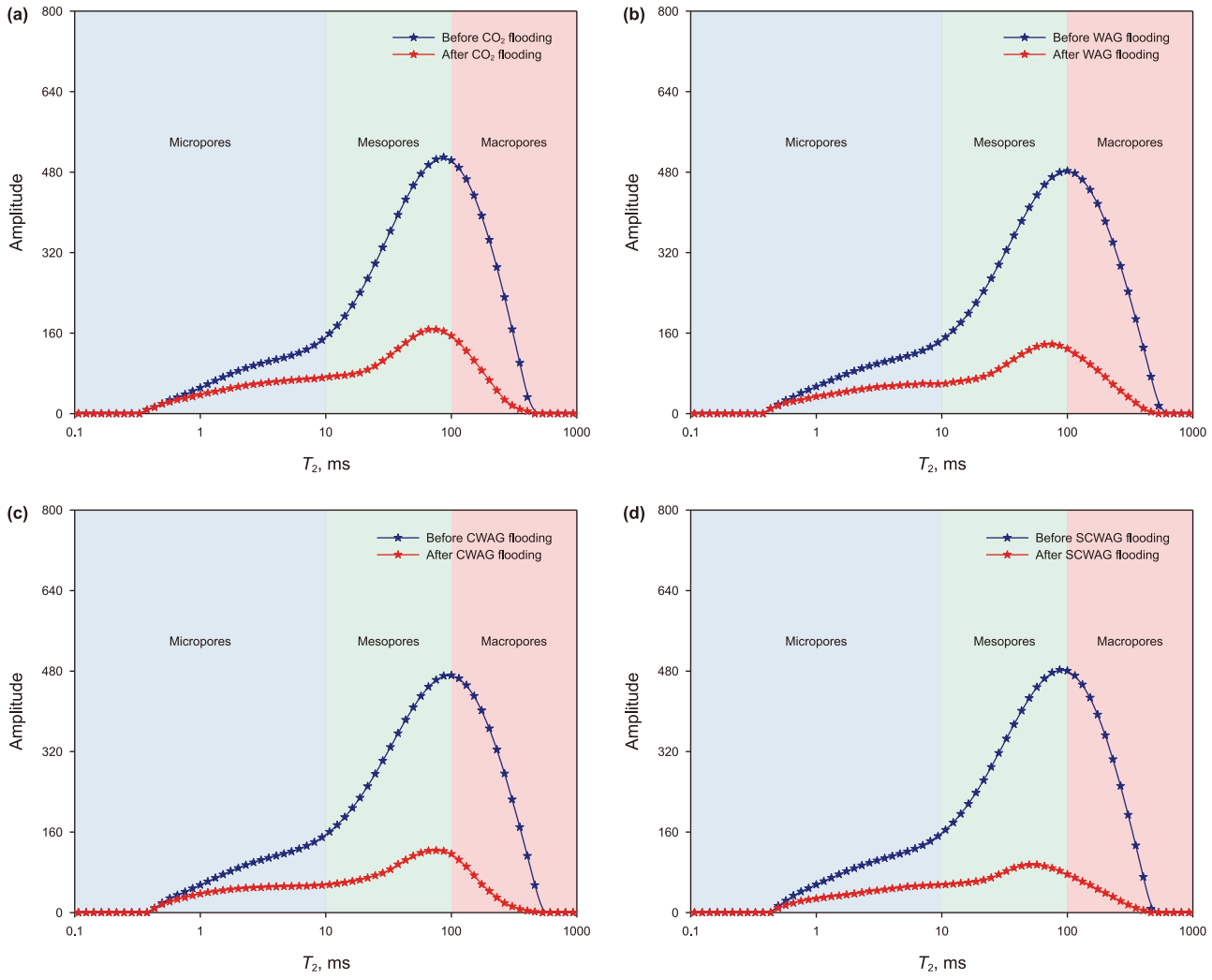

Fig. 5. NMR T_2 spectra before and after experiments with different displacement methods. **(a)** CO_2 flooding; **(b)** WAG flooding; **(c)** CWAG flooding; **(d)** SCWAG flooding.

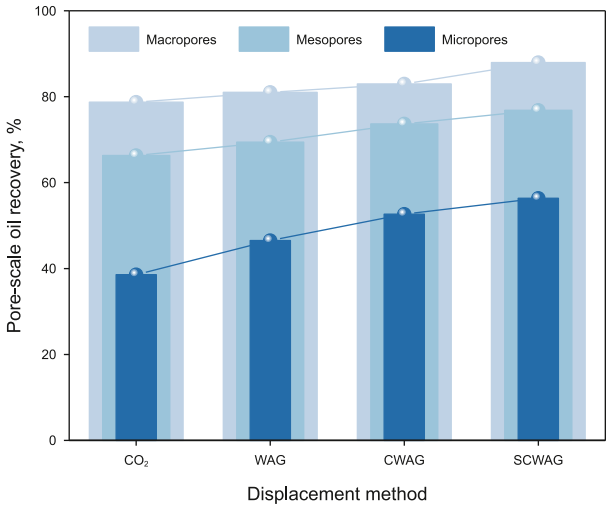

Fig. 6. Recovery comparison by pore type for different displacement methods.

(Nowrouzi et al., 2019). As shown in Fig. 8, following CWAG flooding, the contact angle decreased from 129.6° to 97.1°. In contrast, SCWAG flooding significantly improved wettability, reducing the contact angle from 135.2° to 49.5°. Consequently, SCWAG enables SCW to penetrate smaller core pores and contact oil, thereby facilitating CO_2 mass transfer and improving microscopic sweep efficiency and oil displacement efficiency. Furthermore, the acidic environment generated by SCW could protonate the zwitterionic surfactant, potentially leading to enhanced adsorption at the oil-water interface and on the rock surface, further improving wettability and reducing IFT (Sarkar et al., 2021).

2.4.2. CO_2 storage efficiency

Fig. 9 provides a comparison of CO_2 storage efficiency across CO_2 flooding, WAG flooding, CWAG flooding, and SCWAG flooding. Among these, CO_2 flooding exhibited the lowest storage efficiency at 46.67%, whereas the storage efficiencies of WAG flooding and CWAG flooding were similar, at 55.60% and 54.83%, respectively. SCWAG achieved the highest CO_2 storage efficiency at 57.22%. Owing to the brief core flooding duration and the mineral composition of the core is predominantly quartz, mineralization reactions between CO_2 and the rock can be disregarded (Berndsen et al., 2024; Seyyedi and Sohrabi, 2015). CO_2 flooding primarily occupies reservoir pore space by displacing oil, with a portion of CO_2 dissolving in bound water and residual oil, thereby contributing to CO_2 storage. However, as CO_2 was susceptible to gas breakthrough, a substantial amount of CO_2 was lost at the outlet, resulting in reduced storage efficiency.

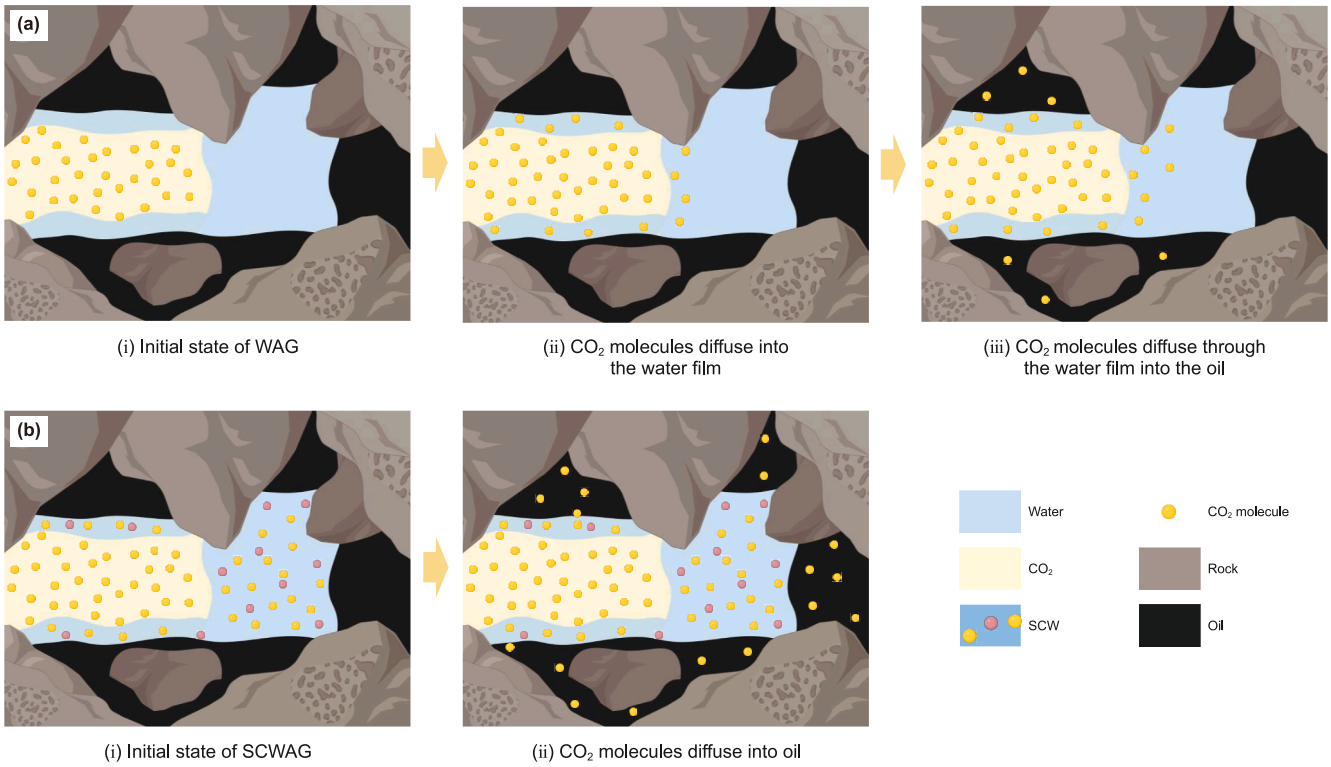

Fig. 7. Schematic illustration of the mechanism by which SCWAG mitigates the water shielding. **(a)** Process of CO_2 transfer to oil during WAG flooding; **(b)** Process of CO_2 transfer to oil during SCWAG flooding.

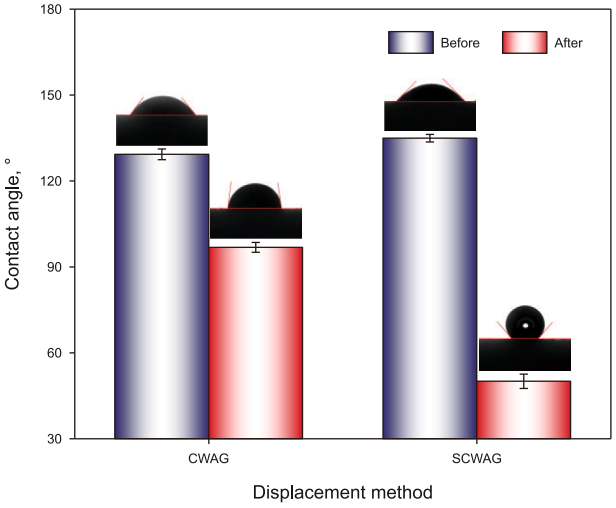

Fig. 8. Comparison of contact angle changes before and after SCWAG and CWAG flooding.

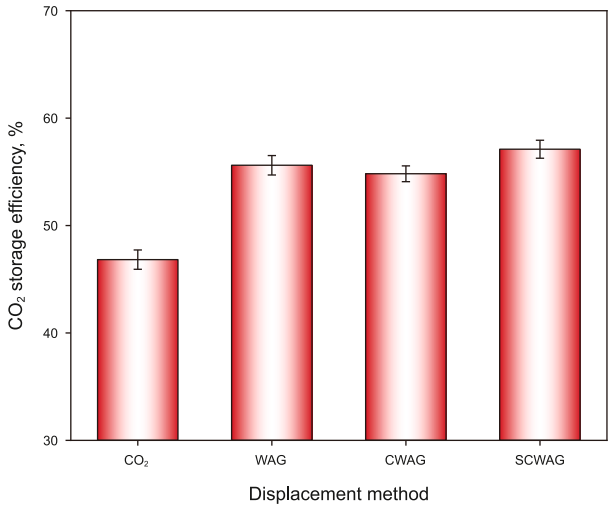

Fig. 9. CO_2 storage efficiency comparison for different displacement methods.

In contrast, WAG flooding stabilized the gas displacement front through alternating injections of water and gas, effectively suppressing gas breakthrough. This enabled more oil to be displaced from core pores, thereby providing increased pore space for CO_2 storage. Furthermore, CO_2 dissolved not only in bound water and residual oil but also in injected water, further enhancing dissolved CO_2 storage in water. Consequently, the CO_2 storage efficiency for WAG flooding significantly increased to 55.60%.

Although CWAG mitigated the effects of water shielding and achieved higher recovery, CO_2 was pre-dissolved in CW, necessitating a larger CO_2 injection volume. Moreover, CW had limited capacity to further dissolve injected CO_2, resulting in a slightly lower CO_2 storage efficiency compared with WAG. SCWAG further enhanced recovery, expanded the pore space available for CO_2 storage, and enhanced CO_2 mass transfer. As a result, CO_2 storage efficiency rose to 57.22%, surpassing both WAG and CWAG.

3. Numerical simulation

3.1. Modeling of carbonated water

The setup for the CW simulation in the numerical simulation software followed the methodology described by Ji et al. (2023).

The key to numerical simulation of CW lies in describing the solubility differences of CO_2 in oil and water, which are determined by the partition coefficient of CO_2 between oil and water (Yang et al., 2019). The CO_2 partition coefficient is defined as the ratio of its effective molar fractions in the oil and water phases, as expressed in Eq. (6) (Li and Nghiem, 1986):

$$\log p = \log \frac{c_o}{c_w} \tag{6}$$

where, c_o and c_w are the CO_2 molar fractions in the oil and water phases, respectively.

The molar fraction of CO_2 in the liquid phase can be expressed using fugacity and Henry's constant, as shown in Eq. (7) (Nghiem et al., 1983):

$$f_{iw} = x_i H_i \tag{7}$$

where, f_{iw} is fugacity of component i in the liquid phase, Pa; x_i is molar fraction of component i; H_i is Henry's constant of component i, Pa.

The Henry's constant is a function of temperature and pressure, which can be calculated using Eq. (8):

$$\ln H_i = \ln H_i^* + \frac{\nu_i (p - p^*)}{RT} \tag{8}$$

where, p^* is reference pressure,Pa; H_i^* is value of Henry's constant at p^*, Pa; T is temperature, K; R is ideal gas constant, J/(mol^{-1}·K^{-1}).

Under the isothermal condition, H_i^* for CO_2 can be calculated using Eq. (9) (Harvey, 1996):

$$\ln(H_i^*) = \ln({p_{H_2O}}^*) - A(T_{H_2O})^{-1} + B(1 - T_{r,H_2O})^{0.355}(T_{r,H_2O})^{-1} + C\exp(1 - T_{r,H_2O})(T_{r,H_2O})^{-0.41} \tag{9}$$

where, ${p_{H_2O}}^*$ is saturated vapor pressure of water, MPa; T_{r,H_2O} is reduced temperature of water, K. A, B, and C are constants, A = −9.4234, B = 4.0087, C = 10.3199.

3.2. Establishment of numerical simulation model

3.2.1. Compositional numerical model

Numerical simulations were performed using the compositional model in CMG. The constituent compounds of oil were lumped into pseudo-components to enhance computational efficiency. The parameters of the resulting pseudo-component model were tuned to match the experimental data from constant composition expansion, multi-stage differential liberation, gas expansion, and minimum miscibility pressure experiments. These experimental data adequately captured the intrinsic properties of the crude oil and the interactions between CO_2 and the oil. The fitting results are shown in Fig. 10(a)–(e), demonstrating excellent agreement between the experimental and simulation data. It is noteworthy that the fitting of the minimum miscibility pressure was achieved by integrating PVT fitting with numerical slim tube simulations. Furthermore, the phase diagrams of the pseudo-components and full components were compared (Fig. 10(f)). At the reservoir temperature, the corresponding saturation pressures were 9.529 and 9.509 MPa for the complete composition and pseudo-component model, respectively. These values closely approximated the actual saturation pressure of 9.532 MPa in the target block, with the pseudo-component model exhibiting a saturation pressure error of 0.24%. This comprehensive validation confirmed that the pseudo-component lumping scheme was both accurate and reliable for subsequent numerical simulations. The specific compositions and characteristic parameters of the pseudo-components are presented in Table 2.

3.2.2. History matching

SCW refers to CW supplemented with surfactants. Therefore, in addition to simulating the transport process of CO_2, it is essential to adjust the relative permeability curves to accurately reflect the effects of both components, thereby enabling the simulation of SCW (Kumar et al., 2021; Lee et al., 2017, 2020). Consequently, a numerical simulation at the experimental scale was established, and the results of laboratory experiments were fitted to refine the relative permeability curves for subsequent reservoir-scale numerical simulation studies. To account for the impact of core heterogeneity on SCWAG flooding and to derive more precise relative permeability curves through history matching, a 3D heterogeneous numerical simulation model reflecting the actual physical properties of the core was constructed using CT scanning. The formula for calculating porosity is presented as Eq. (10) (Akin and Kovscek, 2003):

$$\phi = \frac{CT_{oil} - CT_{air}}{CT_o - CT_a} \tag{10}$$

where CT_{oil}, CT_{air}, CT, and CT_a represent the CT values of oil-saturated cores, air-saturated cores, oil, and air, respectively.

The porosity of the C-4 core is 0.157, and the corresponding permeability is calculated based on the Kozeny-Carman equation as Eq. (11) (Lyu et al., 2021):

$$k = \alpha \frac{\phi^3 D_p^2}{(1 - \phi)^2} \tag{11}$$

where, k is core permeability, mD; α is the proportionality and unity factor, mD/mm^2; D_p is average grain size of rock particles, mm; ϕ is core porosity.

The CT scan results are shown in Fig. 11(a), from which the actual porosity distribution was obtained. To enhance the computational efficiency of the model, it was appropriately coarsened, namely resampled. The resampled results are shown in Fig. 11(b). The porosity distribution after resampling closely aligned with the actual core porosity distribution, thereby ensuring the validity and accuracy of the simulation. The resampled data were then utilized to construct a 3D heterogeneous numerical simulation model. The grid sizes in the x, y, and z directions are 13.023, 6.258, and 6.258 × 10^{-2} cm, respectively, with a total of 98,483 grid blocks.

Based on this numerical simulation model, the injection rate, experimental temperature and pressure were set to align with laboratory experiments. The relative permeability curves were refined, and the CMOST module was utilized to fit the experimental data through history matching. The endpoints of the relative permeability curves, determined from experimental measurements, were kept fixed during the history matching process. The results of history matching, as depicted in Fig. 12, indicate an error of 2.12% relative to the experimental data, suggesting that incorporating the CO_2 partition coefficient in the oil-water system together with history matching enables an accurate simulation of SCWAG. The fitted relative permeability curves are presented in Fig. 13 for use in subsequent reservoir-scale numerical simulation studies.

3.2.3. Reservoir-scale model description

To evaluate the impact of various factors on SCWAG flooding and CO_2 storage efficiency, and to quantify their sensitivities, a

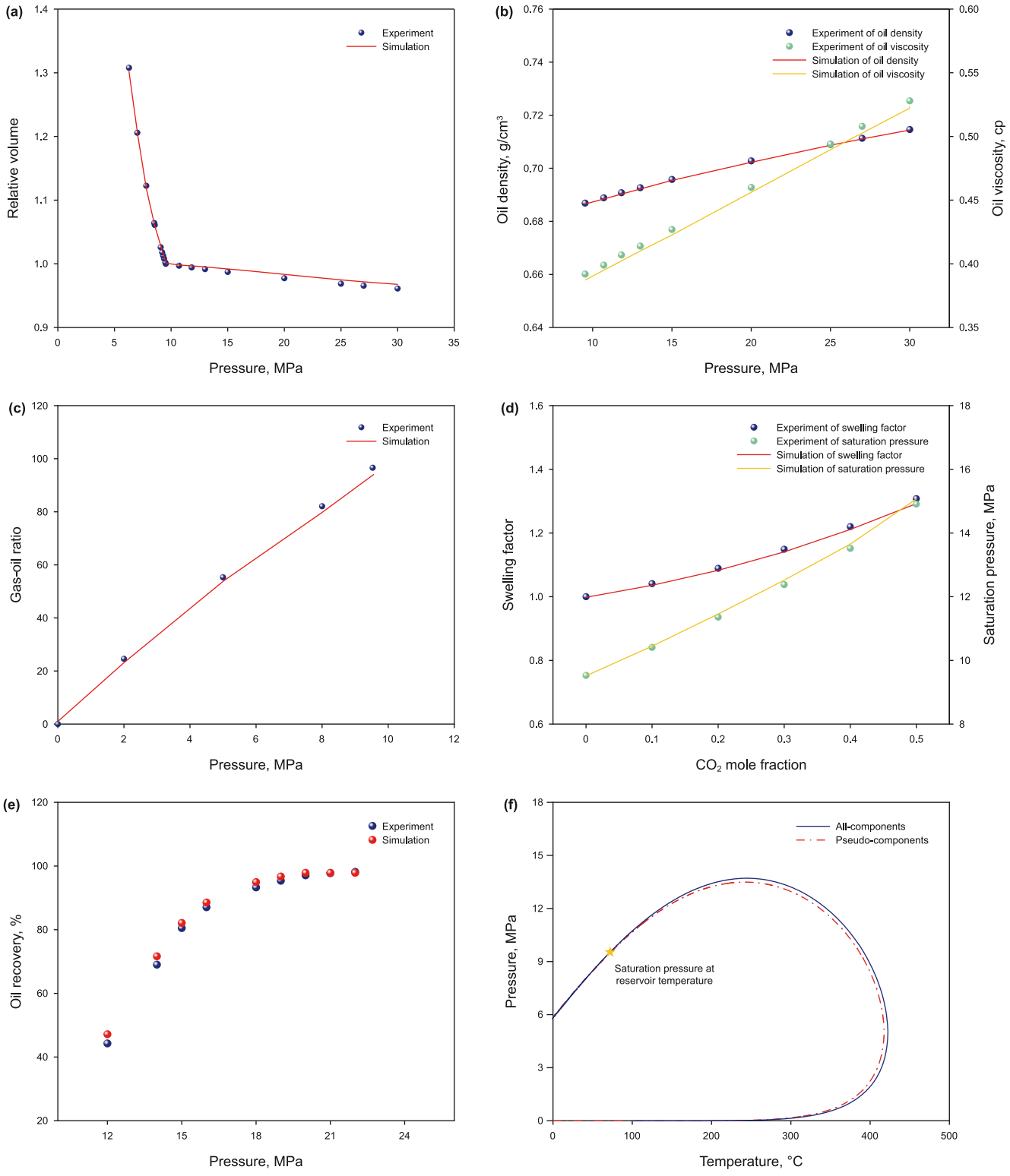

Fig. 10. Fitting results for oil properties and its interaction with CO_2. **(a)** Relative volume; **(b)** Density and viscosity; **(c)** Multistage degassing gas-oil ratio; **(d)** Swelling factor and saturation pressure; **(e)** Minimum miscibility pressure; **(f)** Pressure-temperature phase diagrams.

reservoir-scale numerical simulation model was developed and numerical simulations were conducted, with the ultimate aim of providing a reference for the application of SCWAG in low-permeability reservoirs. The specific parameters of the model, including porosity, permeability, pressure, and temperature, are detailed in Table 3. To reflect the impact of heterogeneity, the model incorporates a permeability contrast of 5, designating the upper layer as a low-permeability zone and the lower layer as a high-permeability zone. The simulation employed a quarter five-spot pattern, consisting of one injection well and one production

Table 2
Composition and properties of pseudo-components.

Component	Mole fraction, %	Molecular weight, g·mol^{-1}	V_c, mol^{-1}	P_c, atm	T_c, K	Acentric factors	Z_c
N_2	0.918	28.013	0.0895	33.5	126.2	0.04	0.291
CO_2	0.071	44.010	0.094	72.8	304.2	0.225	0.274
CH_4	26.045	16.043	0.099	45.4	190.6	0.008	0.288
C_2H_6	6.579	30.070	0.148	48.2	305.4	0.098	0.279
C_3H_8	9.386	44.097	0.203	41.9	369.8	0.152	0.276
C_4 to C_7	20.598	72.481	0.302	34.393	471.614	0.241	0.272
C_8 to C_{14}	17.792	156.940	0.561	23.639	639.809	0.472	0.269
C_{15} to C_{21}	13.784	288.409	0.916	15.887	758.988	0.747	0.27
C_{22} to C_{29}	4.646	336.715	1.187	12.307	824.753	0.942	0.242
C_{30} to C_{32}	0.182	399.601	1.423	9.982	876.687	1.094	0.229

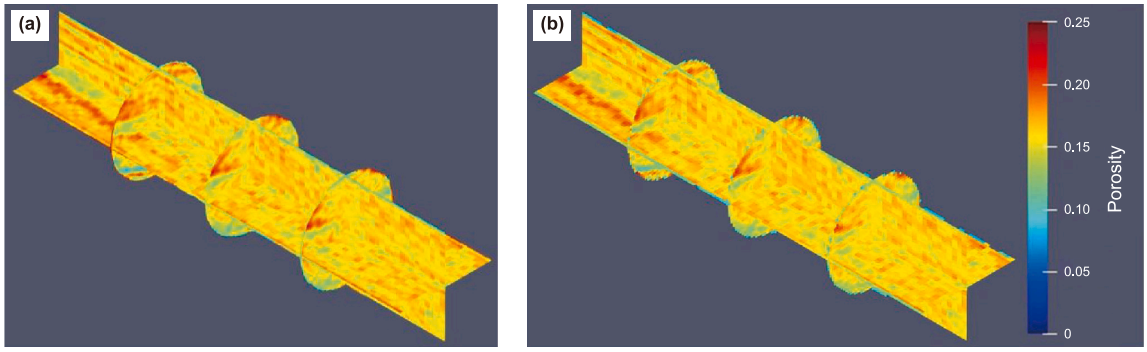

Fig. 11. Comparison of porosity distribution. **(a)** CT scanning; **(b)** Resampling.

well. One complete alternating cycle between SCW and CO_2 was set to 6 months. The injection well operates under constant-rate injection, with a daily injection volume of 18 m^3 under reservoir conditions. The production well was constrained by a minimum bottom-hole pressure of 10 MPa and a daily fluid production rate of 18 m^3.

3.3. Design of simulation schemes

The impacts of injection rate, water-to-gas ratio, and permeability contrast on SCWAG oil recovery and CO_2 storage efficiency were examined. In the single-factor analysis, only one factor was varied, while the other two were held constant. The simulation schemes are presented in Table 4. Given the limited quantitative analysis in existing studies regarding the effects of each factor on recovery and CO_2 storage efficiency, and the absence of research on factor interactions, RSM was employed to quantify the influence of the three factors on SCWAG recovery and CO_2 storage efficiency, while accounting for interactions among the factors. Injection rate (A), water-to-gas ratio (B), and permeability contrast (C) were selected as input variables for the RSM central composite design. The three variables and their respective levels are presented in Table 5.

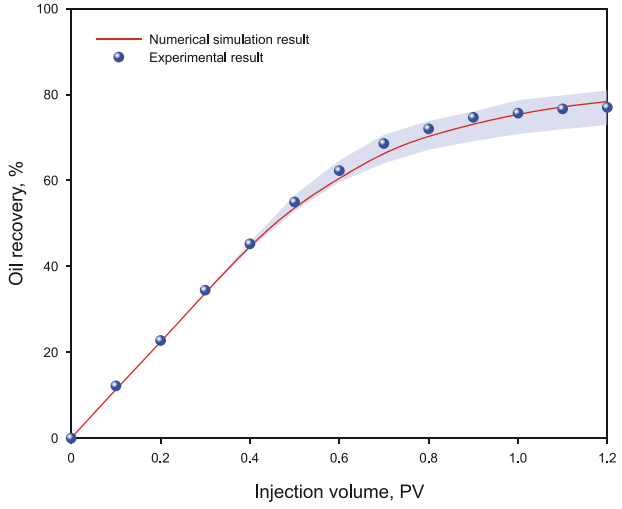

Fig. 12. Experimental and numerical simulation fitting results.

3.4. Simulation results analysis

3.4.1. Single-factor analysis

(1) Injection rate

Fig. 14 illustrates the variation in oil recovery and CO_2 storage efficiency with injection rate. As the injection rate increased, SCWAG recovery rose, while CO_2 storage efficiency decreased. Specifically, when the injection rate increased from 14 m^3/day to 22 m^3/day, recovery increased from 54.37% to 58.24%, whereas CO_2 storage efficiency decreased from 72.74% to 48.23%. The increase in gas injection rate results in a higher total injection volume, which enhanced oil displacement and, consequently, improved recovery. However, a high injection rate also increased viscous forces, which could destabilize the displacement front and increase the likelihood of gas breakthrough, leading to a significant decrease in CO_2 storage efficiency. Optimizing the injection rate is necessary to maximize both oil recovery and CO_2 storage efficiency. Additionally, the economic implications of high injection volumes should be considered when implementing this process in the field.

(2) Water-to-gas ratio

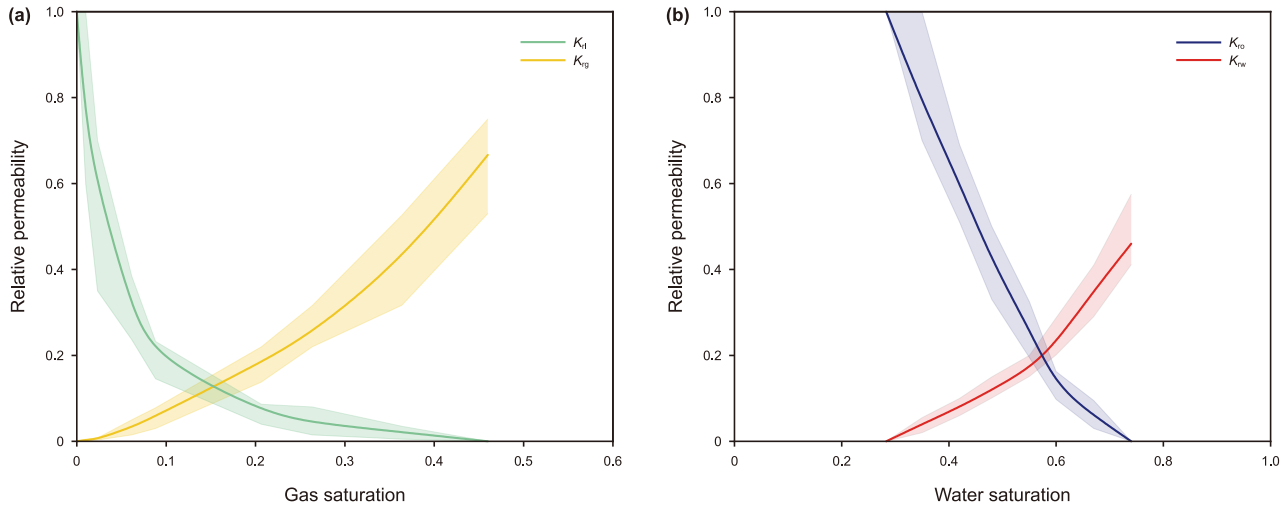

Fig. 13. Relative permeability curves fitted by CMOST. **(a)** Gas-liquid relative permeability; **(b)** Oil-water relative permeability.

The recovery and CO_2 storage efficiency results at different water-to-gas ratios are shown in Fig. 15. As the water-to-gas ratio increased, both recovery and CO_2 storage efficiency increased. When the water-to-gas ratio increased from 1:2 to 2:1, recovery increased from 54.47% to 57.09%, and CO_2 storage efficiency increased markedly from 48.93% to 72.12%. An increase in the water-to-gas ratio enhanced the control of water over the gas, which helped stabilize the gas displacement front. Additionally, it facilitated CO_2 dissolution and storage in water, thus increasing both oil recovery and CO_2 storage efficiency.

It is important to note that although this study showed that a water-to-gas ratio of 2:1 yielded better results than ratios of 1:1 and 1:2, a higher ratio is not always better. When the water-to-gas ratio is markedly low, the control of SCW over CO_2 is insufficient, causing CO_2 to form a continuous phase and result in gas breakthrough, leading to low sweep efficiency (Lewis et al., 2008; Wang et al., 2020). For instance, in the simulations, defining gas breakthrough by a gas-oil ratio of 1500 m^3/m^3. Under this criterion, the 2:1 water-to-gas ratio delayed breakthrough by one year compared to the 1:2 ratio. Conversely, when the water-to-gas ratio is too high, the efficiency of oil displacement is reduced. Therefore, in practical reservoir development, the optimal water-to-gas ratio should be selected based on the specific characteristics of the reservoir.

Table 3
The properties of the reservoir model for the SCWAG simulation.

Parameter	Value
Average porosity, %	16.0
Average permeability, mD	15.0
Initial oil saturation, %	70.0
Grid block in *x*, *y*, *z* directions	50, 50, 6
Dimensions (*x*, *y*, *z*), m	5.64, 5.64, 3.0
Top depth, m	2200.0
Original formation pressure, MPa	25.0
Initial temperature, °C	72.0

Table 4
The simulation schemes of single-factor analysis.

Parameter	Scheme of simulation	Basic parameter value
Injection rate, m^3/d	14, 16, 18, 20, 22	18
Water-to-gas ratio	1:2, 1:1.5, 1:1, 1.5:1, 2:1	1:1
Permeability contrast	2, 3.5, 5, 6.5, 8	5

Table 5
Input variables and levels for RSM.

Factor	Variable	Levels	
		Low	High
Injection rate, m^3/d	A	14	22
Water-to-gas ratio	B	0.5	2
Permeability contrast	C	2	8

(3) Permeability contrast

Fig. 16 illustrates the variations in oil recovery and CO_2 storage efficiency across different permeability contrasts. As the permeability contrast increases, recovery gradually decreases, whereas CO_2 storage efficiency initially increases before subsequently decreasing. A lower permeability contrast corresponds to weaker reservoir heterogeneity, which delays gas breakthrough and leads to higher oil recovery. However, the simulation model represented a positive rhythm reservoir. To ensure a controlled comparison, the overall permeability of the model was kept constant, while only the permeability contrast was varied. The smaller permeability contrast implied a relatively higher vertical permeability in the

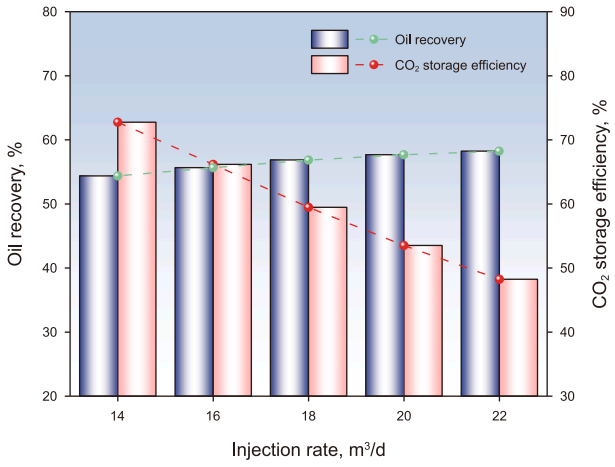

Fig. 14. Variation of recovery and CO_2 storage efficiency with injection rate.

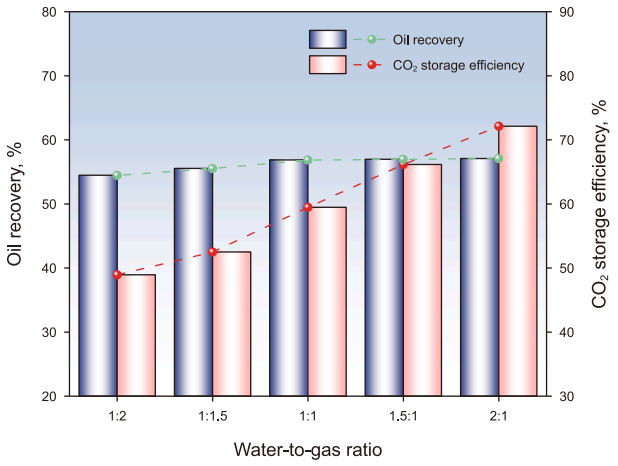

Fig. 15. Variation of recovery and CO_2 storage efficiency with water-to-gas ratio.

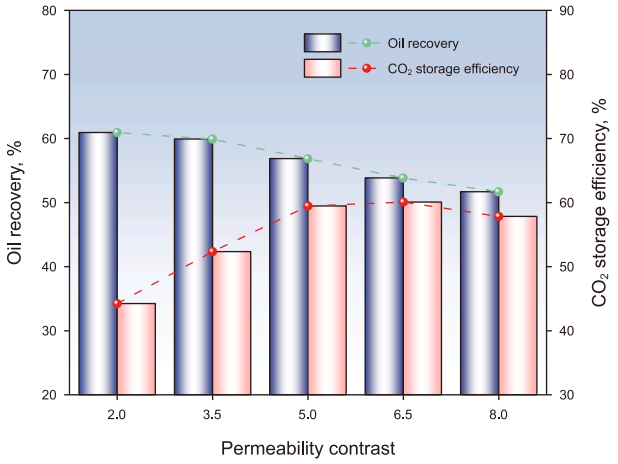

Fig. 16. Variation of recovery and CO_2 storage efficiency with permeability contrast.

upper part of the reservoir; therefore, cases with low permeability contrast were more susceptible to gravity override. As the permeability contrast increased from 2.0 to 6.5, gas breakthrough was delayed compared to the highest-contrast case, but the gas-oil ratio rose rapidly post-breakthrough. Consequently, while the oil recovery decreased from 60.94% to 53.84%, the CO_2 storage efficiency increased from 44.23% to 60.08%. However, upon a further increase in permeability contrast to 8.0, the intensified heterogeneity led to an earlier gas breakthrough, and as a result, both oil recovery and CO_2 storage efficiency declined to 51.69% and 57.83%, respectively. Therefore, the influence of permeability contrast on oil recovery and CO_2 storage efficiency is complex. To optimize oil recovery while achieving effective CO_2 storage, it is crucial to thoroughly consider the complex influences of permeability contrast on both oil recovery and CO_2 storage efficiency.

3.4.2. Sensitivity analysis

The P-values of the response surface analysis models for recovery (Y_1) and CO_2 storage efficiency (Y_2) were less than 0.001. Typically, a P-value below 0.05 indicates that the factor or model is statistically significant. Therefore, these models exhibited high statistical significance, excellent fit, and practical applicability. A scatter plot comparing predicted and actual values is shown in Fig. 17, where the close alignment further validates the reliability of the model. The F-value quantifies the contribution of each variable to the model, with a higher F-value indicating a greater influence of the corresponding factor (Afari et al., 2022). Generally, there is a correlation between the P-value and F-value, whereby a larger F-value corresponds to a smaller P-value.

Based on the F-values, the influencing factors were ranked, and significant factors were identified in conjunction with the P-values, as illustrated in Fig. 18. Factors A, B, and C each exerted a significant influence on both recovery (Y_1) and CO_2 storage efficiency (Y_2), underscoring the appropriateness of the selected factors and affirming their critical roles in governing SCWAG performance. However, the extent of influence of A, B, and C varied between recovery and CO_2 storage efficiency. For Y_1, the influence hierarchy was C > A > B, with permeability contrast indicative of heterogeneity, directly regulating the timing of gas breakthrough and impacting oil displacement efficiency, thereby exerting the most substantial effect on oil recovery. For Y_2, the influence hierarchy shifted to A > B > C, where the injection rate slightly outweighed the water-to-gas ratio in influence, while permeability contrast had a lesser impact compared to the other two factors. The injection rate and water-to-gas ratio directly govern the CO_2 injection volume, significantly affecting CO_2 storage efficiency. Consequently, to maximize oil recovery, the impact of permeability contrast should be prioritized, whereas optimizing CO_2

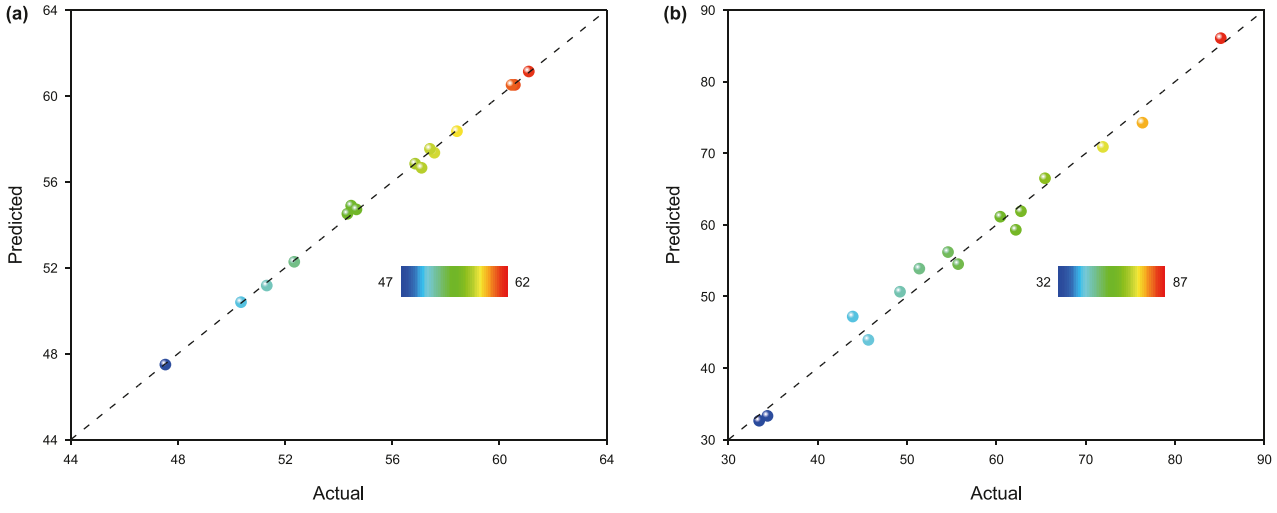

Fig. 17. Scatter plot comparing predicted and actual values. **(a)** Oil recovery; **(b)** CO_2 storage efficiency.

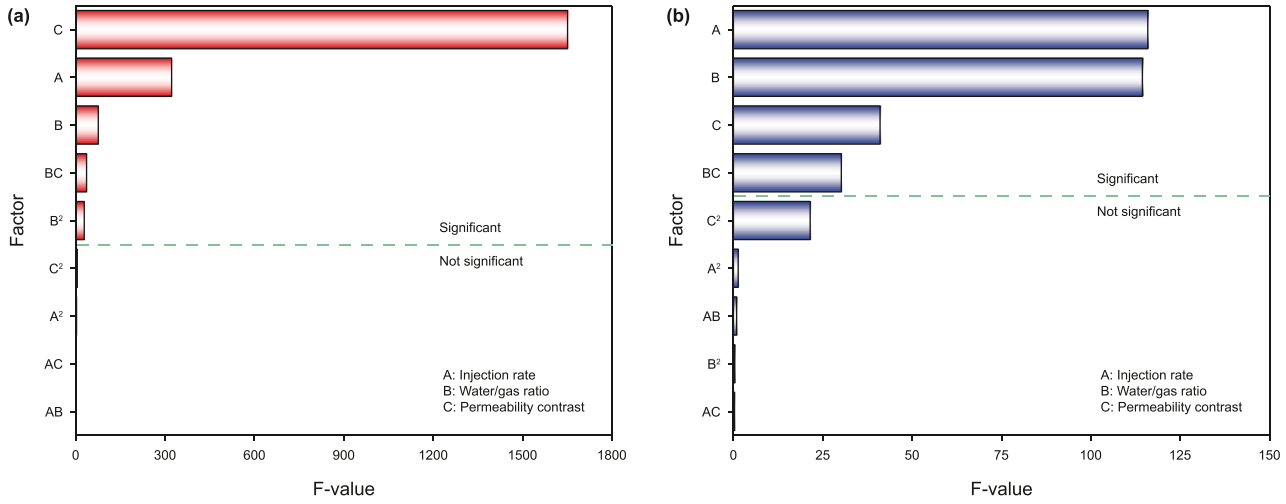

Fig. 18. Ranking of factors by impact degree and significance assessment. **(a)** Oil recovery; **(b)** CO_2 storage efficiency.

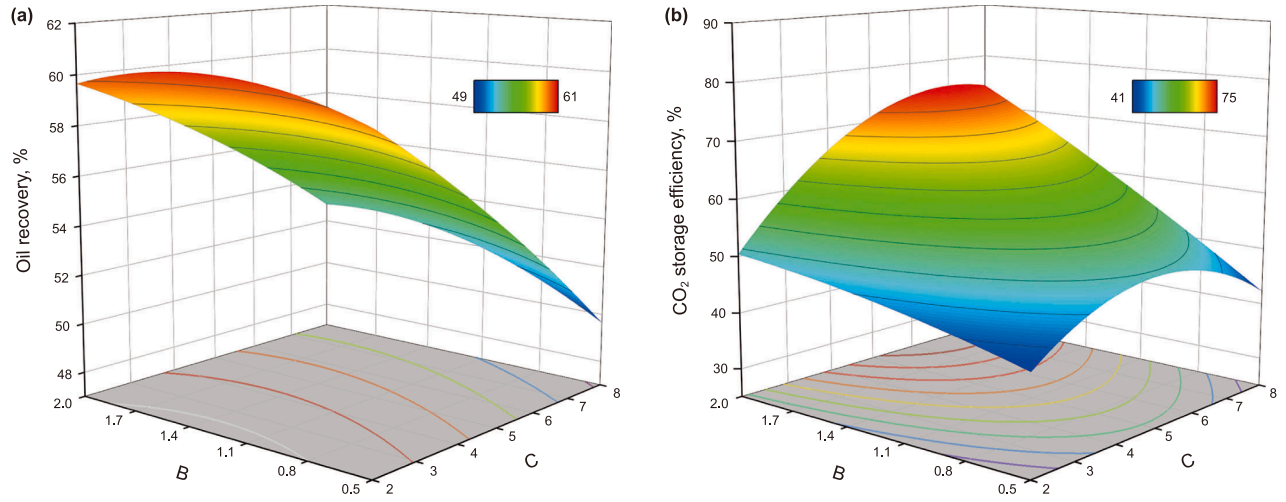

Fig. 19. Response surface plots of interaction between water-to-gas ratio (B) and permeability contrast (C). **(a)** Oil recovery; **(b)** CO_2 storage efficiency.

storage efficiency requires focusing primarily on the injection rate and water-to-gas ratio.

Given the substantial influence of the interaction between the water-to-gas ratio and permeability contrast on both oil recovery and CO_2 storage efficiency, and their predominant effect among interacting factors, response surface plots for oil recovery and CO_2 storage efficiency as functions of factors B and C are presented in Fig. 19. When permeability contrast remained constant, both oil recovery and CO_2 storage efficiency increased with an increasing water-to-gas ratio. Compared to low permeability contrast, the impact of the water-to-gas ratio on recovery and CO_2 storage efficiency was more pronounced at high permeability contrast. A greater permeability contrast signifies enhanced reservoir heterogeneity, necessitating a corresponding increase in the water-to-gas ratio to mitigate gas breakthrough. With a constant water-to-gas ratio, an increase in permeability contrast led to a gradual initial decrease in oil recovery, followed by a sharp decline, whereas CO_2 storage efficiency initially rose before subsequently falling. At lower water-to-gas ratios, permeability contrast exerted a more pronounced effect on both recovery and CO_2 storage efficiency, with this effect diminishing at higher water-to-gas ratios. A higher water-to-gas ratio can partially mitigate the adverse impacts of reservoir heterogeneity; however, when permeability contrast becomes excessively high, even a higher water-to-gas ratio still results in substantial reductions in both oil recovery and CO_2 storage efficiency. This suggests that merely increasing the water-to-gas ratio is insufficient to effectively manage gas breakthrough, and that it cannot be increased indefinitely. Consequently, under conditions of high permeability contrast, integrating SCW with gels, foams, or other techniques may be necessary to more effectively counteract the detrimental effects of reservoir heterogeneity (Kumar and Mandal, 2017; Sun et al., 2024; Tan et al., 2024; Zhao et al., 2024).

4. Conclusion

Although SCWAG demonstrates potential for improved oil recovery, the current understanding of its performance and mechanisms remains insufficient. By employing core flooding experiments and NMR scanning, this study provides the first elucidation of pore-scale oil displacement characteristics and CO_2 storage performance of SCWAG. Furthermore, by integrating CT scanning with numerical simulation, and employing RSM, the influences of various factors and their interactions on SCWAG

performance have been thoroughly investigated. The findings provide new insights into the underlying mechanisms and offer crucial guidance for the design and implementation of SCWAG.

(1) SCWAG flooding integrates the advantages of surfactants, CW, and CO_2. It not only suppresses gas channeling but also effectively mitigates the effect of water shielding. The zwitterionic surfactant and CW could mutually enhance each other, significantly improving wettability, reducing IFT, and promoting CO_2 mass transfer, thus facilitating EOR. The recovery of SCWAG is 76.99%, with recoveries for micropores, mesopores, and macropores of 56.35%, 76.85%, and 87.96%, respectively. The contribution of mesopores and macropores to recovery is substantial, while the improvement in micropores is particularly significant when compared to CO_2 flooding.

(2) WAG flooding improves sweep efficiency, with CO_2 dissolving in trapped water, residual oil, and the injected water. The CO_2 storage efficiency was 55.60%, which was 8.93% higher than that of CO_2 flooding. Although CWAG helps alleviate the impact of water shielding and facilitates CO_2 mass transfer into oil, CW is less effective at continuously dissolving the injected CO_2, resulting in slightly lower CO_2 storage efficiency compared to WAG flooding. SCWAG, on the other hand, provides a larger pore space for CO_2 storage and further promoted CO_2 mass transfer, achieving a CO_2 storage efficiency of 57.22%.

(3) A higher injection rate results in a larger injection volume, which is beneficial for improving recovery. However, a high injection rate is detrimental to maintaining the stability of the displacement front, leading to a decrease in CO_2 storage efficiency. As the water-to-gas ratio increases, SCW more effectively controls CO_2 flow, which is beneficial for improving both recovery and CO_2 storage efficiency. The impact of permeability contrast on SCWAG is complex. As permeability contrast increases, recovery declines, while the CO_2 storage efficiency initially increases and then decreases, as observed within the parameter range of this study.

(4) Injection rate, water-to-gas ratio, and permeability contrast have a significant impact on both recovery and CO_2 storage efficiency, but their relative effects vary for each objective. Permeability contrast has the greatest impact on recovery, exceeding both the injection rate and water-to-gas ratio. In contrast, CO_2 storage efficiency is primarily influenced by the injection rate, which has a slightly greater impact than the water-to-gas ratio and a more pronounced impact than permeability contrast. Beyond these individual factors, the interaction between the water-to-gas ratio and permeability contrast should also be considered in SCWAG for low-permeability reservoirs.

Overall, SCWAG offers a promising approach to EOR and CO_2 storage through its ability to improve sweep efficiency and enhance oil displacement. Future research could explore the potential of integrating SCW with other agents, such as gels and foams, to improve its adaptability and performance in highly heterogeneous reservoirs. Furthermore, it would be worthwhile to investigate the development of novel surfactants that enhance CO_2 solubility in water and facilitate CO_2 mass transfer, potentially leading to further improvements in SCWAG performance.

CRediT authorship contribution statement

Xiao-Bing Han: Writing – original draft, Methodology, Investigation. **Hai-Yang Yu:** Writing – review & editing, Investigation, Conceptualization. **Tong-Bing Wang:** Visualization, Software, Methodology. **Peng Song:** Validation, Resources, Conceptualization. **Jia-Bang Song:** Visualization, Software. **Lu Liu:** Visualization, Methodology, Formal analysis. **Hui-Ting Tang:** Validation, Methodology, Investigation. **Jun Lu:** Validation, Methodology, Formal analysis. **Yang Wang:** Writing – review & editing, Methodology.

Declaration of interests

The authors declare that they have no known competing financial interests or personal relationships that could have appeared to influence the work reported in this paper.

Acknowledgments

This work was financially supported by the National Science and Technology Major Project (2025ZD1406204) and the National Natural Science Foundation of China (52074317).

References

Afari, S., Ling, K., Sennaoui, B., et al., 2022. Optimization of CO_2 huff-n-puff EOR in the Bakken Formationusing numerical simulation and response surface methodology. J. Petrol. Sci. Eng. 215, 110552. https://doi.org/10.1016/j.petrol.2022.110552.

Afzali, S., Rezaei, N., Zendehboudi, S., 2018. A comprehensive review on Enhanced oil recovery by water alternating gas (WAG) injection. Fuel 227, 218–246. https://doi.org/10.1016/j.fuel.2018.04.015.

Akin, S., Kovscek, A.R., 2003. Computed tomography in petroleum engineering research. Geological Society 215 (1), 23–38. https://doi.org/10.1144/GSL.SP.2003.215.01.03.

Alabdulbari, O.A.A., Alabid, F.S.R., Hosseini, S., 2022. Effects of formation brine, [C_{12}mim] [Cl] concentration, temperature and pressure on the swelling factor and IFT of the carbonated water/heavy crude oil system. Braz. J. Chem. Eng. 39 (1), 289–300. https://doi.org/10.1007/s43153-021-00210-6.

Bai, M.X., Zhang, Z.C., Yang, E.L., et al., 2025. Experimental study of microscopic oil production and CO_2 storage in low-permeable reservoirs. Pet. Sci. 22 (2), 756–770. https://doi.org/10.1016/j.petsci.2024.12.015.

Berndsen, M., Erol, S., Akın, T., et al., 2024. Experimental study and kinetic modeling of high temperature and pressure CO_2 mineralization. Int. J. Greenh. Gas Control 132, 104044. https://doi.org/10.1016/j.ijggc.2023.104044.

Chen, X.X., Paprouschi, A., Elveny, M., et al., 2021. A laboratory approach to enhance oil recovery factor in a low permeable reservoir by active carbonated water injection. Energy Rep. 7, 3149–3155. https://doi.org/10.1016/j.egyr.2021.05.043.

Cui, J.L., Zheng, M., Bian, Z.H., et al., 2024. Elevated CO_2 levels promote both carbon and nitrogen cycling in global forests. Nat. Clim. Change 14, 511–517. https://doi.org/10.1038/s41558-024-01973-9.

Dong, M., Foraie, J., Huang, S., et al., 2005. Analysis of immiscible water-alternating-gas (WAG) injection using micromodel tests. J. Can. Petrol. Technol. 44 (2), 17–25. https://doi.org/10.2118/05-02-01.

Filonchyk, M., Peterson, M.P., Zhang, L.F., et al., 2024. Greenhouse gases emissions and global climate change: examining the influence of CO_2, CH_4, and N_2O. Sci. Total Environ. 935, 173359. https://doi.org/10.1016/j.scitotenv.2024.173359.

Gao, X.Y., Yang, S.L., Wang, B.D., et al., 2025. Pore-scale modeling of multiple fluids flow transport kinetics for CO_2 enhanced gas recovery. Energy 315, 134486. https://doi.org/10.1016/j.energy.2025.134486.

Golkari, A., Riazi, M., 2018. Comparative study of oil spreading characteristics for water and carbonated water systems using live and dead oils. J. Petrol. Sci. Eng. 171, 242–252. https://doi.org/10.1016/j.petrol.2018.07.034.

Han, X.B., Yu, H.Y., Wu, Y.H., et al., 2025. Experimental investigation on the countercurrent imbibition distance and factors influencing the imbibition recovery of carbonated fracturing fluid. SPE J. 30, 1474–1491. https://doi.org/10.2118/218205-PA.

Hao, H.D., Zhao, F.L., Hou, J.R., et al., 2016. Parameter optimization for enhanced oil recovery: Mechanisms of WAG flooding in heterogeneous low permeability layers. Petrol. Sci. Bull. 1 (2), 233–240. https://doi.org/10.3969/j.issn.2096-1693.2016.02.019.

Harvey, A.H., 1996. Semiempirical correlation for Henry's constants over large temperature ranges. AIChE J. 42 (5), 1491–1494. https://doi.org/10.1002/aic.690420531.

He, L., Ren, S.K., Zhang, H., 2023. Fingering crossover and enhanced oil recovery mechanism of water-alternating-CO_2 injection. Phys. Fluids 35 (5), 053322. https://doi.org/10.1063/5.0150075.

He, L., Zhao, F.Y., He, W.J., et al., 2024. Fingering inhibition triggered by CO_2 dissolution and viscosity reduction in water-alternating-CO_2 injection. Int. J. Heat Fluid Flow 110, 109646. https://doi.org/10.1016/j.ijheatfluidflow.2024.109646.

Ji, M., Kwon, S., Choi, S., et al., 2023. Numerical investigation of CO_2-carbonated water-alternating-gas on enhanced oil recovery and geological carbon storage. J. CO2 Util. 74, 102544. https://doi.org/10.1016/j.jcou.2023.102544.
Kumar, S., Mandal, A., 2017. A comprehensive review on chemically enhanced water alternating gas/CO_2 (CEWAG) injection for enhanced oil recovery. J. Petrol. Sci. Eng. 157, 696–715. https://doi.org/10.1016/j.petrol.2017.07.066.
Kumar, N., Pal, N., Mandal, A., 2021. Nanoemulsion flooding for enhanced oil recovery: theoretical concepts, numerical simulation and history match. J. Petrol. Sci. Eng. 202, 108579. https://doi.org/10.1016/j.petrol.2021.108579.
Lee, J.H., Jeong, M.S., Lee, K.S., 2017. Geochemical modelling of carbonated low salinity water injection CLSWI to improve wettability modification and oil swelling in carbonate reservoir. In: SPE Latin America and Caribbean Mature Fields Symposium. https://doi.org/10.2118/184915-MS.
Lee, Y., Kim, S., Wang, J., et al., 2020. Relationship between oil production and CO_2 storage during low-salinity carbonate water injection in acid carbonate reservoirs. J. Ind. Eng. Chem. 88, 215–223. https://doi.org/10.1016/j.jiec.2020.04.016.
Lewis, E., Dao, E.K., Mohanty, K.K., 2008. Sweep efficiency of miscible floods in a high-pressure quarter-five-spot model. SPE J. 13 (4), 432–439. https://doi.org/10.2118/102764-PA.
Li, Y.K., Nghiem, L.X., 1986. Phase equilibria of oil, gas and water/brine mixtures from a cubic equation of state and henry's law. Can. J. Chem. Eng. 64 (3), 486–496. https://doi.org/10.1002/cjce.5450640319.
Lin, Q.Y., Zhang, X., Wang, T., et al., 2022. Technical perspective of carbon capture, utilization, and storage. Engineering 14, 27–32. https://doi.org/10.1016/j.eng.2021.12.013.
Liu, Y.L., Rui, Z.H., 2022. A storage-driven CO_2 EOR for a net-zero emission target. Engineering 18, 79–87. https://doi.org/10.1016/j.eng.2022.02.010.
Liu, J.R., Zhang, D.F., Liu, S.Y., et al., 2025. Multiscale investigation into EOR mechanisms and influencing factors for CO_2-WAG injection in heterogeneous sandy conglomerate reservoirs using NMR technology. Pet. Sci. 22 (7), 2977–2991. https://doi.org/10.1016/j.petsci.2025.04.004.
Luo, X.J., Wei, B., Gao, K., et al., 2023. Gas channeling control with an in-situ smart surfactant gel during water-alternating-CO_2 enhanced oil recovery. Pet. Sci. 20 (5), 2835–2851. https://doi.org/10.1016/j.petsci.2023.03.003.
Lyu, X.C., Voskov, D., Tang, J.Y., et al., 2021. Simulation of foam enhanced-oil-recovery processes using operator-based linearization approach. SPE J. 26 (4), 2287–2304. https://doi.org/10.2118/205399-PA.
Majidaie, S., Khanifar, A., Onur, M., et al., 2012. A simulation study of chemically enhanced water alternating gas CWAG injection. In: SPE EOR Conference at Oil and Gas West Asia. https://doi.org/10.2118/154152-MS.
Nghiem, L.X., Aziz, K., Li, Y.K., 1983. A robust iterative method for flash calculations using the soave-redlich-kwong or the Peng-Robinson equation of state. Soc. Petrol. Eng. J. 23 (3), 521–530. https://doi.org/10.2118/8285-PA.
Nowrouzi, I., Manshad, A.K., Mohammadi, A.H., 2019. Effects of dissolved carbon dioxide and ions in water on the dynamic interfacial tension of water and oil in the process of carbonated smart water injection into oil reservoirs. Fuel 243, 569–578. https://doi.org/10.1016/j.fuel.2019.01.069.
Nowrouzi, I., Mohammadi, A.H., Manshad, A.K., 2020. Utilization of methanol and acetone as mutual solvents to reduce interfacial tension (IFT) in enhanced oil recovery process by carbonated smart water injection. J. Mol. Liq. 304, 112733. https://doi.org/10.1016/j.molliq.2020.112733.
Ren, B., Duncan, I.J., 2021. Maximizing oil production from water alternating gas (CO_2) injection into residual oil zones: the impact of oil saturation and heterogeneity. Energy 222, 119915. https://doi.org/10.1016/j.energy.2021.119915.
Riazi, M., Golkari, A., 2016. The influence of spreading coefficient on carbonated water alternating gas injection in a heavy crude oil. Fuel 178, 1–9. https://doi.org/10.1016/j.fuel.2016.03.021.
Sarkar, R., Pal, A., Rakshit, A., et al., 2021. Properties and applications of amphoteric surfactant: a concise review. J. Surfactants Deterg. 24 (5), 709–730. https://doi.org/10.1002/jsde.12542.
Seyyedi, M., Sohrabi, M., 2015. Enhancing water imbibition rate and oil recovery by carbonated water in carbonate and sandstone rocks. Energy & Fuels 30 (1), 285–293. https://doi.org/10.1021/acs.energyfuels.5b02644.
Seyyedi, M., Sohrabi, M., Sisson, A., et al., 2018. Quantification of oil recovery efficiency, CO_2 storage potential, and fluid-rock interactions by CWI in heterogeneous sandstone oil reservoirs. J. Mol. Liq. 249, 779–788. https://doi.org/10.1016/j.molliq.2017.10.070.
Shakiba, M., Ayatollahi, S., Riazi, M., 2016. Investigation of oil recovery and CO_2 storage during secondary and tertiary injection of carbonated water in an Iranian carbonate oil reservoir. J. Petrol. Sci. Eng. 137, 134–143. https://doi.org/10.1016/j.petrol.2015.11.020.
Shu, G.L., Dong, M.Z., Chen, S.N., et al., 2014. Improvement of CO_2 EOR performance in water-wet reservoirs by adding active carbonated water. J. Petrol. Sci. Eng. 121, 142–148. https://doi.org/10.1016/j.petrol.2014.07.001.
Song, J.B., Yu, H.Y., Han, X.B., et al., 2025. Oil displacement and CO_2 storage mechanisms of impure CO_2 flooding in tight reservoirs: insights from microfluidic experiments and numerical simulations. Fuel 393, 134934. https://doi.org/10.1016/j.fuel.2025.134934.
Sun, X.F., Ning, H.Y., Chen, G.P., et al., 2024. Experimental study of hybrid nanofluid-alternating-CO_2 microbubble injection as a novel method for enhancing heavy oil recovery. J. Mol. Liq. 395, 123835. https://doi.org/10.1016/j.molliq.2023.123835.
Tan, X.H., Ma, X.J., Li, X.P., et al., 2024. An adsorption model considering fictitious stress. Fract. Fract. 9, 17. https://doi.org/10.3390/fractalfract9010017.
Tang, M.R., Wang, C.W., Deng, X.A., et al., 2022. Experimental investigation on plugging performance of nanospheres in low-permeability reservoir with bottom water. Adv. Geo-Energy Res. 6 (2), 95–103. https://doi.org/10.46690/ager.2022.02.02.
Tiffin, D.L., Yellig, W.F., 1983. Effects of Mobile water on multiple-contact miscible gas displacements. Soc. Petrol. Eng. J. 23 (3), 447–455. https://doi.org/10.2118/10687-PA.
Vo Thanh, H., Sugai, Y., Nguele, R., et al., 2020. Robust optimization of CO_2 sequestration through a water alternating gas process under geological uncertainties in Cuu Long Basin, Vietnam. J. Nat. Gas Sci. Eng. 76, 103208. https://doi.org/10.1016/j.jngse.2020.103208.
Wang, L., He, Y.M., Wang, Q., et al., 2020. Multiphase flow characteristics and EOR mechanism of immiscible CO_2 water-alternating-gas injection after continuous CO_2 injection: A micro-scale visual investigation. Fuel 282, 118689. https://doi.org/10.1016/j.fuel.2020.118689.
Xiao, P.F., Yang, Z.M., Wang, X.W., et al., 2017. Experimental investigation on CO_2 injection in the Daqing extra/ultra-low permeability reservoir. J. Petrol. Sci. Eng. 149, 765–771. https://doi.org/10.1016/j.petrol.2016.11.020.
Yang, P., Guo, H.K., Yang, D.Y., 2013. Determination of residual oil distribution during waterflooding in tight oil formations with NMR relaxometry measurements. Energy & Fuels 27 (10), 5750–5756. https://doi.org/10.1021/ef400631h.
Yang, Z.L., Yu, H.Y., Chen, Z.W., et al., 2019. A compositional model for CO_2 flooding including CO_2 equilibria between water and oil using the Peng–Robinson equation of state with the Wong–Sandler mixing rule. Pet. Sci. 16, 874–889. https://doi.org/10.1007/s12182-018-0294-2.
Yu, H.Y., Rui, Z.H., Chen, Z.W., et al., 2019. Feasibility study of improved unconventional reservoir performance with carbonated water and surfactant. Energy 182, 135–147. https://doi.org/10.1016/j.energy.2019.06.024.
Yu, H.Y., Chen, Z.W., Lu, X., et al., 2020. Review of enhanced oil recovery by carbonated water injection. Petrol. Sci. Bull. 5 (2), 204–228. https://doi.org/10.3969/j.issn.2096–1693.2020.02.019.
Yu, H.Y., Fu, W.R., Zhang, Y.P., et al., 2021. Experimental study on EOR performance of CO_2-based flooding methods on tight oil. Fuel 290, 119988. https://doi.org/10.1016/j.fuel.2020.119988.
Zhang, X., Wei, B., You, J.Y., et al., 2021. Characterizing pore-level oil mobilization processes in unconventional reservoirs assisted by state-of-the-art nuclear magnetic resonance technique. Energy 236, 121549. https://doi.org/10.1016/j.energy.2021.121549.
Zhang, X.C., Luo, Z.X., Liu, J.L., et al., 2023. Experimental evaluation of the water-based enhanced oil recovery methods in ultra-tight reservoirs. J. Pet. Explor. Prod. Technol. 13 (9), 1911–1918. https://doi.org/10.1007/s13202-023-01655-w.
Zhao, Y., Wen, X., Rui, Z.H., et al., 2024. A novel dual-network CO_2-responsive particle gel for mitigating CO_2 channeling and leakage in hydrocarbon recovery and carbon storage. Chem. Eng. J. 498, 155187. https://doi.org/10.1016/j.cej.2024.155187.
Zhou, C., Richardson-Barlow, C., Fan, L.Y., et al., 2025. Towards organic collaborative governance for a more sustainable environment: evolutionary game analysis within the policy implementation of China's net-zero emissions goals. J. Environ. Manag. 373, 123765. https://doi.org/10.1016/j.jenvman.2024.123765.